Influence of charged-dislocation density variations on carrier mobility in heteroepitaxial semiconductors: The case of SnO_2 on sapphire

S. K. Vasheghani Farahani,[1] T. D. Veal,[2,*] A. M. Sanchez,[1] O. Bierwagen,[3,4] M. E. White,[3] S. Gorfman,[1,†] P. A. Thomas,[1] J. S. Speck,[3] and C. F. McConville[1,‡]

[1]*Department of Physics, University of Warwick, Coventry CV4 7AL, United Kingdom*

[2]*Stephenson Institute for Renewable Energy, School of Physical Sciences, University of Liverpool, Liverpool L69 4ZF, United Kingdom*

[3]*Materials Department, University of California, Santa Barbara, California 93106-5050, USA*

[4]*Paul-Drude-Institut für Festkörperelektronic, Hausvogteiplatz 5-7, D-10117 Berlin, Germany*

(Received 29 May 2012; published 17 December 2012)

In highly mismatched heteroepitaxial systems, the influence of carrier- and dislocation-density variations on carrier mobility is revealed. Transmission electron microscopy reveals the variation of dislocation density through a series of SnO_2 films grown by molecular-beam epitaxy on sapphire substrates where the lattice mismatch exceeds 11%. A layer-by-layer parallel conduction treatment of the carrier mobility in SnO_2 epilayers is used to illustrate the dominant role of the depth-dependent dislocation density and charge profile in determining the film-thickness dependence of the transport properties.

DOI: 10.1103/PhysRevB.86.245315 PACS number(s): 73.40.−c, 61.72.Ff, 68.35.Dv, 72.10.Fk

I. INTRODUCTION

The electronic properties of oxide heterointerfaces have become an extremely interesting area in materials research, ranging from insulating[1] and semiconducting heterostructures[2] to interface engineering of systems for solid-state electronics.[3,4] Interface-induced defects in lattice-mismatched heterostructures can significantly alter the electronic properties of the films. In heteroepitaxial systems with large lattice mismatch, the crystalline quality, transport, and electronic properties of the films are strongly dependent on film thickness due to the creation of strain relieving misfit and threading dislocations (TDs) originating at the interface. This directly impacts the mobility of the free carriers and the associated device performance. Moreover, as charged dislocations act as a source of free carriers, they make an additional contribution to the conductivity of heterostructures; therefore, the trade-off between carrier density enhancement and limited mobility by dislocations relies on understanding these mutual effects, charging and defect scattering, in heteroepitaxial semiconductor layers.

Several studies have investigated strain relaxation,[5,6] defect reduction,[7–9] and the electrical properties of TDs in highly lattice-mismatched heteroepitaxial III-V materials, including III-nitrides. Indeed, cross-sectional transmission electron microscopy (TEM) and x-ray diffration (XRD) studies on epitaxial GaN[10,11] have shown that dislocations originate at the interface and their density decreases with increasing layer thickness. Somewhat surprisingly, studies of the influence of dislocations on carrier transport properties almost invariably assume a uniform density of dislocations throughout the film. For example, theoretical and experimental work by Look *et al.*[12] and Weimann *et al.*[13] investigating the mobility of carriers in GaN considered a uniform density of dislocations and concluded that the dislocations in GaN are negatively charged. In studies of highly lattice-mismatched MBE-grown InN on sapphire with a GaN buffer layer, dislocations were found to be positively charged, contributing to both the *n*-type conductivity[14,15] and carrier scattering.[16] Modeling of the electrothermal transport data from InN by Miller *et al.*[17] supported the charged nature of dislocations concluded by the previous studies,[12,13] but still took constant values for the dislocation density. However, a recent multilayer analysis of MBE-grown InN using both Hall and Seebeck profiling[18] showed a strong depth-dependence of both the carrier concentration and mobility. In previous studies, a constant or average dislocation density and carrier concentration has been used for each sample. If charged-dislocation scattering is important, then carrier and dislocation density variations throughout the sample must be taken into account as the scattering strength and its variation across the layers for ionized defects are not the same as those for the dislocation deformation potential. Therefore, without a layer-by-layer mobility analysis, no accurate numerical modeling and recognition of the relative effectiveness of these scattering mechanisms would be possible.

In spite of their use as transparent conductors and potential for transparent electronics,[19] relatively little is known about the intrinsic properties of the binary oxide semiconductors. A quasilinear band structure in transparent conducting oxides inferred from a recent orbital tight-binding approach[20] accounts for some changing features in the mobility of ZnO films as a function of carrier concentration. In particular, SnO_2 is an *n*-type transparent conducting oxide with a wide, direct fundamental band gap. It has a significant number of applications in solid-state gas sensing, transparent conducting contacts and electronics, display systems, and as an oxidation catalyst.[21–24] High-quality SnO_2 has only been available as heteroepitaxial films and is therefore subject to interface-induced extended defects. In this work, the mobility of electrons in unintentionally doped highly lattice-mismatched SnO_2/Al_2O_3 films is modeled as a function of carrier concentration within the framework of a layer-by-layer analysis. The most probable scattering mechanisms, i.e., longitudinal polar-optical mode, acoustic deformation potential, ionized defect, acoustic piezoelectric, neutral impurity, and dislocation deformation potential scattering, are all taken into account and the dominant mechanisms identified. We demonstrate that the TDs in MBE-grown SnO_2 on *r*-sapphire are positively charged. This, and the effect of defect scattering, necessitates consideration of the dislocation density and the corresponding

carrier concentration variation as a function of depth for accurate carrier transport studies of highly lattice-mismatched semiconductor materials.

II. EXPERIMENTAL DETAILS

In this study, high-quality, unintentionally doped SnO_2 (101) films, with a range of thicknesses, were grown by plasma-assisted molecular-beam epitaxy (PAMBE) on *r*-plane $(10\bar{1}2)$ sapphire.[25] A standard Knudsen effusion cell was used to evaporate liquid Sn and a Veeco UNI-Bulb radio-frequency plasma source to supply monatomic oxygen. The lattice mismatch of $SnO_2(101)/r$-sapphire samples is 0.4% and -11.3% along the $\langle 010\rangle$ and $\langle 101\rangle$ directions, respectively.

Optical reflectance measurements in the mid-infrared (MIR) region were performed using a Bruker Vertex 70v Fourier-transform infrared (FTIR) spectrometer to determine the thickness of the samples. Because SnO_2 is optically anisotropic, a zinc-selenide MIR polarizer was employed to attain *s*-polarized light. X-ray diffraction (XRD) measurements were implemented to ascertain the $[10\bar{1}]$ direction in the SnO_2 films to align the *s*-polarized electric field $\boldsymbol{E}$ perpendicular to the *c* axis. The crystallographic direction $[10\bar{1}]$ in SnO_2 is aligned with $[\bar{2}\bar{1}1]$ in sapphire. This ensures that by suitable rotation around the surface normal, *s*-polarized light is perpendicular to the *c* axis of SnO_2 and sapphire during the passage of light through the sample. Dislocation analysis was carried out using images acquired under bright field conditions in a Jeol 2000FX TEM. Cross-sectional images were used to determine both the number of dislocations and the depth at which they occur. These values were substantiated by plan-view TEM images in excellent agreement with the cross-sectional values for dislocation densities. Planar defects were also observed with much lower abundance and limited to areas close to the interface. Hall effect measurements based on the standard Van der Pauw geometry were carried out to determine the total sheet density and transport mobility of each sample. All measurements were performed at room temperature.

III. DISLOCATION DENSITY AND CARRIER CONCENTRATION VARIATIONS

A cross-sectional TEM image of the thickest SnO_2/r-sapphire sample is shown in Figs. 1(a) and 1(b). High densities of TDs are observed originating from the interface propagating towards the surface of the film. This interfacial region is expanded in panel (b) showing TDs up to 110 nm from the interface. Dislocation densities as a function of depth (distance from the interface) were obtained from both cross-sectional and plan-view TEM images at specific thicknesses. These data with an exponential fit (solid line) are shown in Fig. 1(c). The data points clearly indicate the depth dependence of the dislocation density, although it becomes increasingly difficult to accurately assess close to the interface, as reflected in the error bars.

Mid-IR *s*-polarized reflectance measurements, satisfying the condition $\boldsymbol{E}\perp\boldsymbol{c}$, were performed at an incident angle of 56° with respect to the surface normal within the range of 50 to 600 meV, to determine the thickness of each sample. The reflectance data were simulated using a 3-layer stratified medium, i.e., vacuum/SnO_2/sapphire with coherent interference. A complex dielectric function was used wherein the transverse and longitudinal polar-optical lattice modes were accounted for within the factorized model with Lorentzian broadening,[26] and the carrier response by the classical Drude model. The sample thicknesses range from 26 to 1505 nm consistent with the values obtained from scanning electron microscopy and TEM. The Hall carrier concentration for each sample was calculated via $n_{\mathrm{av}}^{\mathrm{3D}} = n_{\mathrm{H}}/t$, where n_{H} is the sheet density and t is the thickness of the film.

The Hall carrier concentration shows a significant decrease, and the mobility a comparable increase, with sample thickness,[27] as can be seen in Fig. 1(d). The rapid decrease of carrier concentration with SnO_2 thickness and dislocation density with depth implies that there exists a correlation between carrier concentration and dislocation density indicating the donor-like nature of the TDs. To further corroborate this, modeling of the electron mobility as a function of carrier concentration has been performed. However, the raw Hall data provide an "average" value of both quantities over the whole thickness of each sample. In order to correct for this effect, a parallel conduction analysis was performed to minimize the Hall-averaging error within the layers.[28]

IV. DEPTH PROFILING AND LAYER-BY-LAYER MOBILITY MODELING

Figure 2 shows schematically the thickest sample assumed to consist of seven layers, wherein the distance between each line and the interface corresponds to each available sample with a certain thickness. The sheet density and mobility of each layer are derived according to Eqs. (1) and (2):

$$n_i = \frac{\left(n_{\mathrm{H},i}\mu_{\mathrm{H},i} - \sum_{j=1}^{i-1} n_j\mu_j\right)^2}{n_{\mathrm{H},i}\mu_{\mathrm{H},i}^2 - \sum_{j=1}^{i-1} n_j\mu_j^2}, \tag{1}$$

$$\mu_i = \frac{n_{\mathrm{H},i}\mu_{\mathrm{H},i}^2 - \sum_{j=1}^{i-1} n_j\mu_j^2}{n_{\mathrm{H},i}\mu_{\mathrm{H},i} - \sum_{j=1}^{i-1} n_j\mu_j}, \tag{2}$$

where $n_{\mathrm{H},i}$ and $\mu_{\mathrm{H},i}$ are the Hall sheet density and mobility of each sample embracing i layers, and n_i and μ_i are the sheet density and mobility of the ith layer, respectively. The carrier concentration of each layer is obtained via $n_{\mathrm{3D},i} = n_i/\Delta d_i$ where Δd_i is the thickness of each layer. It is worthy of mention that having had more samples with closer thicknesses (smaller Δds) would result in the minimization of errors in depth profiling. The mobility and carrier concentration of each layer are represented as $\mu\,(n_{\mathrm{3D}})$ as shown in Fig. 3. The carrier concentration as a function of depth, $n_{\mathrm{3D}}\,(d)$, is determined by fitting a curve to the calculated data points; see Fig. 2(b). Using $n_{\mathrm{3D}}\,(d)$ in the exponential fit shown by the solid line in Fig. 1(c) allows the derivation of carrier concentration variations with dislocation density. This is shown in Fig. 2(b) which signifies the fact that the carrier concentration increases (decreases) with dislocation density (distance from the interface). Hence, a direct link between the dislocation density and carrier concentration is made via parallel conduction and depth analysis in the functional, $N_{\mathrm{dis}}(d\,(n_{\mathrm{3D}}))$, throughout the SnO_2 layers and is used in our mobility modeling.

A layer-by-layer model of mobility versus carrier concentration, $\mu\,(n_{\mathrm{3D}})$, has been performed by accounting for

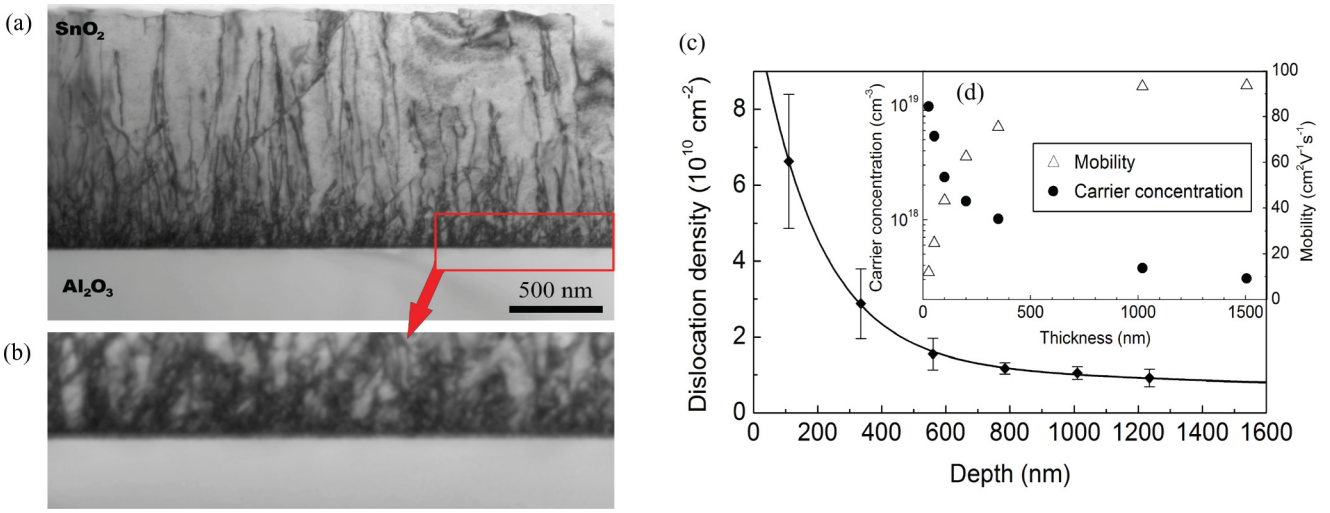

FIG. 1. (Color online) (a) Cross-sectional TEM image of MBE-grown SnO_2/r-sapphire showing the TDs formed at the interface and propagating through the layer. The expansion of the region outlined in red is shown in (b) demonstrating the extremely high dislocation density in the region less than 110 nm from the interface. (c) Corresponding dislocation density profile versus depth (distance from the interface). As the concentration of dislocations is highest close to the interface, there is a higher degree of error in the measured dislocation densities. The solid curve is the exponential fit to the data points. (d) The same trend in (c) is observed for the Hall carrier concentration as a function of thickness contrary to the Hall mobility, which increases with sample thickness.

the key scattering mechanisms, namely, acoustic deformation potential (ADP),[29] acoustic piezoelectric (AP),[30] longitudinal polar-optical mode (LPO),[29,31] neutral impurity (NI),[32] ionized defect (ID),[29,33] and dislocation deformation potential (DDP) scattering.[34] Figure 3 shows the results of the model curves pertaining to successive inclusion of the dominant mobility-limiting scattering mechanisms using the standard Matthiessen rule. This rule has been employed while being aware of the possible error due to an extra term pertaining to possible interdependencies of different scattering mechanisms. Nonetheless, as the modeling is performed at a single temperature, any discrepancy is expected to be only a constant offset of the entire mobility curve, leaving all reported trends intact.

As mentioned earlier, the treatment of optical properties is with respect to the condition $\boldsymbol{E}\perp\boldsymbol{c}$, wherein the longitudinal optical (LO) modes propagate parallel to the surface as well as the carriers. All three LO modes used in mid-IR reflectance simulations have been considered for polar optical scattering. In respect of ionized defect scattering, model carrier statistics have been calculated to evaluate the Fermi level positions using a band gap and band edge effective mass of 3.5 eV[35] and $0.27m_0$[36] (an average value according to the optical and electronic anisotropy of SnO_2) at room temperature, respectively. As the Fermi-level positions corresponding to the layer carrier concentrations range between -0.08 and 0.04 eV with respect to the conduction band minimum, and the charge neutrality level (CNL) of SnO_2 lies 0.5 eV above the CBM,[37] the density of ionized defects has been approximated by that of ionized donors. That is, it has been assumed that the acceptor density is negligible. Moreover, referencing to the Fermi-level positions, it has been deduced from first-principles density functional theory calculations in SnO_2[38,39] that hydrogen impurities and Sn_i (tin interstitial) native defects are the most probable charged defects to form, which are singly and doubly charged, respectively. Both charge states have been considered in modeling the respective scattering mechanisms. As the dependence of carrier concentration on dislocation density is set according to the analyses above, dislocation scattering is treated as a dual mechanism, due to the charged centers and the deformation potential generated by their presence in the lattice. In order to distinguish the relative importance and effectiveness, different expressions have been used for these two mechanisms, contrary to previous works wherein a single expression has been used for charged-dislocation scattering. The scattering by positively charged defects along the dislocations has been accounted for using the Brooks-Herring (BH) formula[29] for carrier concentrations below the Mott transition level for SnO_2, $n = 10^{18}$ cm^{-3}, and the degenerate form of the BH formula[33] for carrier concentrations above the Mott level. Additionally, assuming an isotropic distribution of dislocations, the following relation has been utilized for DDP scattering-limited mobility which explicitly takes into account relevant characteristic parameters such as Poisson's ratio and DDP of the lattice,[34]

$$\mu_{\mathrm{DDP}} = \frac{32K_{\mathrm{B}}T\hbar e}{3\pi E^2 l^2 m^* N_{\mathrm{dis}}}\left(\frac{1-\nu}{1-2\nu}\right)^2, \qquad (3)$$

where ν is the Poisson ratio which is 0.29 for SnO_2,[40] m^* is the effective mass, l is the unit slip distance, and E is the characteristic energy pertaining to the scattering potential; a value of $E = 7$ eV has been used for SnO_2 which lies within the range of the determined values for other materials. The other quantities have their usual meanings. As the lattice mismatch of $SnO_2(101)/r$-sapphire is 0.4% and 11.3% along the $\langle 010\rangle$ and $\langle 101\rangle$ directions, respectively, the majority of dislocations are formed with reference to the $\langle 101\rangle$ direction. This has been reflected in the unit slip distance (l).

Previous modeling of charged-dislocation scattering[12,13,41] explains the increase of the mobility for increasing carrier

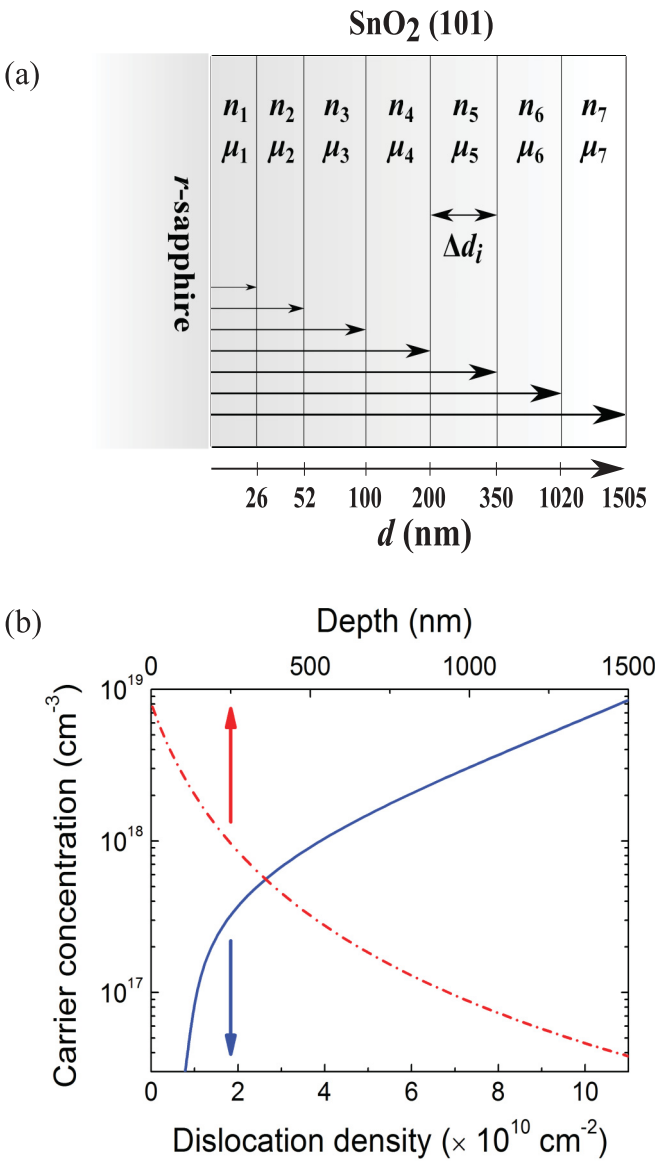

FIG. 2. (Color online) (a) Schematic representation of a 7 layer SnO_2 film on r-sapphire. The area delimited by the interface and every line designates each available sample. Δd_i is the thickness of each layer. (b) A layer-by-layer profile of carrier concentration as a function of dislocation density (solid line) and depth (dot-dashed line); data obtained using parallel conduction analysis together with dislocation density variations with depth.

concentrations up to 10^{17}–10^{18} cm^{-3} as being the result of screened negatively-charged-dislocation scattering in GaN. This increase in mobility is not seen in the case of SnO_2 as the dislocations are positively charged (as shown here). As a result, the screening of positively-charged defects along the dislocations can be treated similarly to that of positively-charged defects in the bulk region within the Brooks-Herring model. This allows a distinctive approach to be employed of independently weighing the dual scattering effect associated with dislocations in heteroepitaxial SnO_2, the deformation potential scattering and the ionized defect scattering associated with the positively-charged defects along the dislocations.

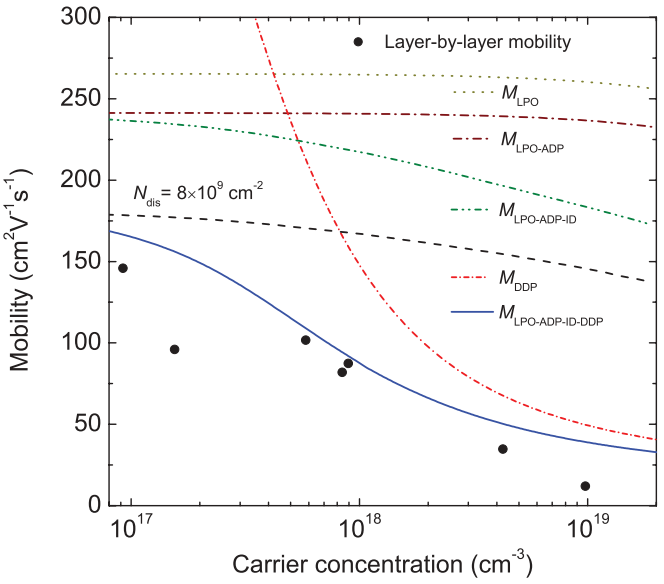

FIG. 3. (Color online) Layer-by-layer mobility versus carrier concentration data and simulation. The model curves resulting from successive addition of the dominant scattering mechanisms using Matthiessen's rule are represented. LPO, ADP, ID, and DDP stand for longitudinal polar-optical mode, acoustic deformation potential, ionized defect, and dislocation deformation potential scattering, respectively. The individual effects of LPO and DDP scattering-limited mobility can be seen in the figure. The dashed line shows the resultant mobility model curve regarding a constant value of $N_{\rm dis} = 8 \times 10^9$ cm^{-2} from the interface to the surface.

From the simulation and analysis of layer-by-layer mobility versus carrier concentration, the highest energy LPO phonon mode is found to interact most strongly with the mobile electrons. As can be seen in Fig. 3, the addition of ADP scattering discernably reduces the mobility. The resultant model curve for LPO and ADP scattering is consistent with the data obtained by Fonstad and Rediker for low carrier density bulk SnO_2.[29] The contribution of ID scattering increases at higher carrier concentrations. If we assume a constant dislocation density at all depths (the value measured for the surface of the thickest sample, $N_{\rm dis} = 8 \times 10^9$ cm^{-2}), the resultant mobility model curve (see the dashed curve in Fig. 3) clearly fails to reproduce the observed decreasing trend of mobility with carrier concentration. Therefore, the effect of the individual DDP scattering-limited mobility model curve, having taken into account the charged-dislocation variations with depth, is plotted representing the drastic mobility change with depth. In this respect, the functional, $N_{\rm dis}(d(n_{\rm 3D}))$, correlating the depth-dependent carrier concentration and dislocation density, has been substituted for $N_{\rm dis}$ in Eq. (3). The resulting model curve closely reproduces the data points, emphasizing the need to include depth-dependent dislocation density as well as carrier concentration variations in transport studies of MBE-grown SnO_2/r-sapphire. Neutral impurity scattering was found to be negligible, and acoustic piezoelectric scattering was found to have only a minor effect on the carriers. This is reasonable given that the rutile SnO_2 lattice possesses an inversion symmetry. In conditions where the CNL is well into the conduction band, as in InN, CdO, and SnO_2, acceptor-type defects are less

likely to form as they tend to be *n* type. Nevertheless, it has been found that self-compensation in InN does take place even for the respective high formation energy levels.[42] Therefore, if there were some acceptor compensation in the SnO_2 samples (which we have assumed to be negligible), it would bring the model curve more towards the data points. Additionally, as the planar defects evidently have much lower abundance in the films and are limited to regions close to the interface, their scattering effect was not considered in the model. This would otherwise improve the model especially towards the tail which corresponds to scattering in the lower layers.

As can be seen in Fig. 3, at carrier concentrations below the Mott transition level of SnO_2, polar optical mode scattering is the dominant mobility-limiting mechanism. Above the Mott level, lattice and ionized defect scattering are all obscured by DDP scattering. Hence, the transport properties are essentially the same for either the singly or doubly charged states of the ionized defects. In highly lattice-mismatched heteroepitaxial materials with charged dislocations and/or grain boundaries, reduction in the screening length due to background doping affecting the mobility of carriers may also be depth dependent.

V. CONCLUSIONS

The depth dependence of carrier concentration and mobility have been shown to be due to TDs in unintentionally doped MBE-grown SnO_2/r-sapphire. Dislocations have been shown to be positively charged and a source of donors, and the significance of their density variations away from the interface towards the surface in respect of electron mobility has been identified. Below the Mott level for SnO_2, the scattering mechanisms are dominated by polar optical mode scattering. The lowering and steep downward trend of mobility toward the SnO_2/r-sapphire interface is well simulated by the dominant effect of DDP scattering as a function of carrier concentration. This observation strongly supports the need to undertake a layer-by-layer analysis and consideration of the variation of charged-dislocation density with depth in carrier mobility studies of highly lattice-mismatched heteroepitaxial semiconductors.

ACKNOWLEDGMENTS

The authors gratefully acknowledge the support of Advantage West Midlands (AWM) and the European Research and Development Fund (ERDF) through the Science City initiative for the facilities used in this research. T.D.V. acknowledges funding from the Engineering and Physical Sciences Research Council, UK, under Grant No. EP/G004447/1. The research at UCSB was supported by the NSF World Materials Network Program (NSF Award No. DMR0909203) and by AFOSR (Kitt Reinhardt and Jim Hwang, Program Managers).

*t.veal@liverpool.ac.uk
†Present address: Department of Physics, University of Siegen, Walter-Flex-Str. 3, 57072, Siegen, Germany.
‡c.f.mcconville@warwick.ac.uk

[1] A. Ohtomo and H. Y. Hwang, Nature (London) **427**, 423 (2004).
[2] B. Höffling, A. Schleife, C. Rödl, and F. Bechstedt, Phys. Rev. B **85**, 035305 (2012).
[3] R. A. McKee, F. J. Walker, and M. F. Chisholm, Science **293**, 468 (2001).
[4] H. W. Jang *et al.*, Science **331**, 886 (2011).
[5] J. G. Belk, J. L. Sudijono, X. M. Zhang, J. H. Neave, T. S. Jones, and B. A. Joyce, Phys. Rev. Lett. **78**, 475 (1997).
[6] A. Ohtake, M. Ozeki, and J. Nakamura, Phys. Rev. Lett. **84**, 4665 (2000).
[7] P. Vennéguès, Semicond. Sci. Technol. **27**, 024004 (2012).
[8] M. D. Craven, S. H. Lim, F. Wu, J. S. Speck, and S. P. DenBaars, Phys. Status Solidi A **194**, 541 (2002).
[9] P. Gibart, Rep. Prog. Phys. **67**, 667 (2004).
[10] J. Jasinski and Z. Liliental-Weber, J. Electron. Mater. **31**, 429 (2002).
[11] A. Reiher, J. Bläsing, A. Dadgar, and A. Krost, Appl. Phys. Lett. **84**, 3537 (2004).
[12] D. C. Look and J. R. Sizelove, Phys. Rev. Lett. **82**, 1237 (1999).
[13] N. G. Weimann, L. F. Eastman, D. Doppalapudi, H. M. Ng, and T. D. Moustakas, J. Appl. Phys. **83**, 3656 (1998).
[14] L. F. J. Piper, T. D. Veal, C. F. McConville, H. Lu, and W. J. Schaff, Appl. Phys. Lett. **88**, 252109 (2006).
[15] V. Cimalla, V. Lebedev, F. M. Morales, R. Goldhahn, and O. Ambacher, Appl. Phys. Lett. **89**, 172109 (2006).
[16] P. D. C. King, T. D. Veal, and C. F. McConville, J. Phys.: Condens. Matter **21**, 174201 (2009).
[17] N. Miller, E. E. Haller, G. Koblmüller, C. Gallinat, J. S. Speck, W. J. Schaff, M. E. Hawkridge, K. M. Yu, and J. W. Ager, Phys. Rev. B **84**, 075315 (2011).
[18] O. Bierwagen, S. Choi, and J. S. Speck, Phys. Rev. B **84**, 235302 (2011).
[19] J. F. Wagner, Science **300**, 1245 (2003).
[20] Y. Kang, S. H. Jeon, Y.-W. Son, Y.-S. Lee, M. Ryu, S. Lee, and S. Han, Phys. Rev. Lett. **108**, 196404 (2012).
[21] E. R. Leite, I. T. Weber, E. Longo, and J. A. Varela, Adv. Mater. **12**, 965 (2000).
[22] A. Goetzberger and C. Hebling, Sol. Energy Mater. Sol. Cells **62**, 1 (2000).
[23] H. Kim, J. S. Horwitz, G. P. Kushto, Z. H. Kafafi, and D. B. Chrisey, Appl. Phys. Lett. **79**, 284 (2001).
[24] M. Batzill and U. Diebold, Prog. Surf. Sci. **79**, 47 (2005).
[25] M. E. White, M. Y. Tsai, F. Wu, and J. S. Speck, J. Vac. Sci. Technol. A **26**, 1300 (2008).
[26] A. Kasic, M. Schubert, S. Einfeldt, D. Hommel, and T. E. Tiwald, Phys. Rev. B **62**, 7365 (2000).
[27] M. E. White, O. Bierwagen, M. Y. Tsai, and J. S. Speck, J. Appl. Phys. **106**, 093704 (2009).
[28] R. L. Petritz, Phys. Rev. **110**, 1254 (1958).
[29] C. G. Fonstad and R. H. Rediker, J. Appl. Phys. **42**, 2911 (1971).
[30] H. T. Grahn, *Introduction to Semiconductor Physics* (World Scientific, 1999).
[31] J. A. Marley and R. C. Dockerty, Phys. Rev. **140**, A304 (1965).

[32]P. P. Debye and E. M. Conwell, Phys. Rev. **93**, 693 (1954).
[33]D. C. Look, H. Lu, W. J. Schaff, J. Jasinski, and Z. Liliental-Weber, Appl. Phys. Lett. **80**, 258 (2002).
[34]D. L. Dexter and F. Seitz, Phys. Rev. **86**, 964 (1952).
[35]D. Fröhlich, R. Kenklies, and R. Helbig, Phys. Rev. Lett. **41**, 1750 (1978).
[36]K. J. Button, C. G. Fonstad, and W. Dreybrodt, Phys. Rev. B **4**, 4539 (1971).
[37]J. Robertson and S. J. Clark, Phys. Rev. B **83**, 075205 (2011).
[38]A. K. Singh, A. Janotti, M. Scheffler, and C. G. Van de Walle, Phys. Rev. Lett. **101**, 055502 (2008).
[39] Çetin Kılıç and Alex Zunger, Phys. Rev. Lett. **88**, 095501 (2002).
[40]M. W. Barsoum, E. N. Hoffman, R. D. Doherty, S. Gupta, and A. Zavaliangos, Phys. Rev. Lett. **93**, 206104 (2004).
[41]H. M. Ng, D. Doppalapudi, T. D. Moustakas, N. G. Weimann, and L. F. Eastman, Appl. Phys. Lett. **73**, 821 (1998).
[42]C. Rauch, F. Tuomisto, P. D. C. King, T. D. Veal, H. Lu, and W. J. Schaff, Appl. Phys. Lett. **101**, 011903 (2012).